NASA TECHNICAL NOTE

NASA TN D-3615

NASA TN D-3615

EFFECT OF DISCONTINUITIES IN SURFACE CATALYTIC ACTIVITY ON LAMINAR HEAT TRANSFER IN ARC-HEATED NITROGEN STREAMS

by Robert E. Sheldahl and Ernest L. Winkler

Ames Research Center
Moffett Field, Calif.

NATIONAL AERONAUTICS AND SPACE ADMINISTRATION • WASHINGTON, D. C. • SEPTEMBER 1966

NASA TN D-3615

EFFECT OF DISCONTINUITIES IN SURFACE CATALYTIC ACTIVITY ON LAMINAR HEAT TRANSFER IN ARC-HEATED NITROGEN STREAMS

By Robert E. Sheldahl and Ernest L. Winkler

Ames Research Center
Moffett Field, Calif.

NATIONAL AERONAUTICS AND SPACE ADMINISTRATION

For sale by the Clearinghouse for Federal Scientific and Technical Information
Springfield, Virginia 22151 – Price $1.00

EFFECT OF DISCONTINUITIES IN SURFACE CATALYTIC ACTIVITY ON LAMINAR HEAT TRANSFER IN ARC-HEATED NITROGEN STREAMS

By Robert E. Sheldahl and Ernest L. Winkler
Ames Research Center

SUMMARY

Heat-transfer rates due to forced convection and recombination of dissociated atoms were measured along the afterbodies of hemisphere-cylinders having various discontinuities in surface catalytic activity. Each nose section, which consisted of a hemisphere and a forward portion of the afterbody, was coated with a material of one catalytic activity. The catalytic activity of the material on the remainder of the afterbody surface was either the same or another value. The tests were performed in high enthalpy streams of partially dissociated nitrogen.

The results, compared with a uniformly catalytic test body, show that the use of a noncatalytic material on the forward region of the body substantially increases the heat-transfer rates to the catalytic afterbody surface. This is in qualitative agreement with the theoretical analysis of Chung, Liu, and Mirels.

INTRODUCTION

It is known that the surface of a flight vehicle can, under certain circumstances, act as a third-body catalyst to increase the aerodynamic heating rate. The catalytic surface recombination in the boundary-layer flow of a frozen, dissociated gas has been analyzed by numerous investigators (refs. 1-7). The analyses indicate the possibility of shielding the stagnation region from the heat transfer due to surface recombination of dissociated atoms by means of a surface material that is not catalytic. In such a nonequilibrium flow, an upstream surface material may affect the heating of the downstream portion of a body. One aspect of this problem has been analyzed in reference 6. The vehicle is considered to have a noncatalytic surface over the upstream portion and a catalytic surface over the afterportion. A substantial increase of heat-transfer rate with position along the afterbody surface is computed. It is the purpose of this investigation to provide experimental data for such bodies and to compare the measurements with the analysis of reference 6.

NOMENCLATURE

a	sonic velocity
C	constant in equation (19)
c	calorimeter specific heat
D	diffusion coefficient
H_t	total enthalpy
h_r	heat of recombination of atoms
k	specific reaction rate constant for catalytic surface
M	Mach number
m	α/α_e
p	pressure
$\dot{q}$	heat-transfer rate
$\dot{q}_c$	convective heat-transfer rate
$\dot{q}_d$	heat-transfer rate due to surface recombinations
$\dot{q}_t$	total heat-transfer rate
R	test body nose radius
r	test body radius normal to stream axis, R sin S/R
S	coordinate position along test body surface measured from the stagnation point
s	transformed coordinate (eq. (19))
T	temperature
t	calorimeter wall thickness
u	velocity
x	coordinate along flat-plate body
y	distance normal to the test body
α	mass fraction of atoms

γ	isentropic exponent
ρ	density
ρ_m	calorimeter material density
θ	time

Subscripts

e	edge of boundary layer
o	stagnation point
1	S/R location on the test body surface of the discontinuity in k_w
un	uniform k_w over the complete test body
w	wall
∞	free-stream condition
Cu-Cu	uniform copper surface over the complete test body.
Cu-SiO	copper nose and silicon monoxide afterbody surface material
SiO-SiO	uniform silicon monoxide surface over the complete test body
SiO-Cu	silicon monoxide nose and copper afterbody surface material

APPARATUS AND METHODS

Facility

The tests were performed in a 10.2-cm-diameter, high energy, supersonic, dissociated nitrogen stream. The stream was generated by the water-cooled arc-jet wind-tunnel facility described in detail in references 7 and 8. The nominal conditions of the free-jet test stream were: frozen Mach number 5.6, static pressure of 3×10^{-4} atm, impact pressure of 0.013 atm, and nitrogen flow rate of 2.5 g/sec. The stream energy of 8 to 20 MJ/kg corresponded to an atom-mass-fraction population from 10 to 35 percent.

Test Bodies

The test body for all the tests was a 1.588-cm-diameter hemisphere-cylinder. Four models were built as shown in figure 1. Two were heat-transfer models, one an impact-pressure model, and the fourth a pressure-distribution model for measuring both impact pressure and the static pressure along the afterbody.

The heat-transfer models were built as shown in figure 1(a). The nose section could be separated from the afterbody at S/R = 2.682. The two heat sink nose sections were plated with electrolytically deposited copper to a thickness of approximately 0.002 cm. Copper has a high specific reaction rate constant and served as the catalytic surface. One of the two was then coated with vacuum-deposited silicon monoxide to serve as a nose section of negligible catalyticity as compared to copper. The two afterbody sections were copper-plated, stainless-steel cylinders 0.051 cm thick. They were instrumented with five chromel-alumel thermocouples at S/R locations of 4, 5.5, 7, 8.5, and 9.5. Again, one of the two afterbody sections was coated with vacuum-deposited silicon monoxide.

The water-cooled impact pressure probe had a single orifice located at the stagnation point whereas the pressure-distribution model had orifices at the stagnation point and at the same S/R location as the thermocouple locations on the heat-transfer models.

Procedure

To obtain axial uniformity of the test-stream impact pressure, the static pressure of the free-jet test stream was balanced against the test chamber static pressure by adjusting a throttle valve in the line between the test chamber and the vacuum pumping system. A mechanical differential pressure gage with a full-scale range of ±1 mm Hg detected the difference between the static pressure of the free jet at the nozzle exit and of the test chamber, and the flow was throttled until the indicated differential pressure became zero.

The impact pressure in the test stream was examined with the hemisphere-cylinder impact probe model (fig. 1(b)) and was found to be uniform within 10 percent along the jet axis over the length later occupied by the afterbody.

The afterbody pressures obtained from the pressure-distribution model were indicated on an oil manometer board and were recorded photographically. The calculated lag time for the pressure-measuring system was about one-half minute. The model was allowed to remain in the stream for several minutes to insure that the manometer had stabilized before data were recorded at various fixed values of enthalpy.

The heat-transfer measurements were carried out in the following manner. The impact-pressure model (fig. 1(b)) was mounted on a traversing mechanism along with the heat-transfer model. After the arc heater was started, the free-jet static pressure was balanced against the nozzle exit pressure with the impact-pressure model in the stream. The arc was extinguished, and the traversing mechanism moved the pressure probe aside and inserted the heat-transfer model into the test position. The heat-transfer model was protected with a clamshell shield; the arc was then reignited and allowed to reach steady-state operation. The shield was quickly removed from the model, and the transient heat-transfer data were recorded. After a predetermined length of time (about 1 second), the arc was automatically extinguished. The throttle valve to the ejectors, the tunnel mass flow rate, and the arc-heater power setting were not changed during this sequence of events. Upon restart, arc power

input would repeat with an error that varied from 2 to 6 percent, but these small discrepancies produced no change in throttle valve setting required to balance the test stream. Thus the tunnel conditions during the heat-transfer test were substantially the same as those that existed during the previous test with the impact-pressure probe.

Afterbody heat-transfer-rate distributions were obtained in the pressure-balanced nitrogen jet for all four possible combinations of nose section and afterbody. Prior to each run the copper portions were polished with a metal polish and then cleaned with grain alcohol, but the silicon monoxide surfaces were not disturbed. The afterbody temperatures, sensed by thermocouples, were recorded as a function of time on an oscillograph. The corresponding heat-transfer rates were evaluated by measurement of the slopes of the temperature-time traces and use of the calorimeter equation:

$$\dot{q} = \frac{dq}{d\theta} = \rho_m c t \frac{dT}{d\theta} \tag{1}$$

The effect of heat conduction along the axial length of the calorimeter (fig. 1(a)) on the measurements was estimated by means of the analysis of Manos and Taylor (ref. 9) and found to be negligible when compared to the effect of radial conduction.

RESULTS AND DISCUSSION

Since aerodynamic heat-transfer rates depend strongly on pressure, efforts were taken to obtain the impact pressure and afterbody wall pressure for the run conditions encountered during the tests. The measured variation of impact pressure at the test location in the jet is shown in figure 2 as a function of the stream total enthalpy. Although the impact pressure varied with the total enthalpy, the ratio of impact pressure to nozzle plenum pressure was a constant 0.0315 over the enthalpy range of the tests.

The experimental pressure distribution along the afterbody of the hemisphere-cylinder test body is shown in figure 3. Also shown for comparison is a theoretical result obtained by the methods of reference 10. The theoretical solution is for a three-dimensional blunt body in a perfect gas with the nominal free-stream flow conditions of the test facility. That the results agree adequately may be taken as an indication that the free-jet test stream was uniform. The pressure distributions were obtained at four different enthalpies but no consistent trend with enthalpy was noted. Distributions for enthalpies higher than 14 MJ/kg were not obtained because of the long run times needed to allow the manometer to stabilize.

The Knudson number, based on the gas conditions at the wall and on the orifice diameter, was 0.18, which is less than 0.4 where slip effects are usually encountered. However, according to reference 11, an orifice effect due to the heat flux to the wall may still exist and would tend to give a measured pressure slightly lower than the actual pressure at the model wall. No orifice correction was applied to the data due to the uncertainty of the size of this correction.

The afterbody heat-transfer-rate data were normalized by means of an analytically determined, equilibrium stagnation-point heat-transfer rate corresponding to the enthalpy and stagnation pressure of each run. All sets of data normalized by the same equilibrium relationship would be expected to display catalytic effects independent of explicit dependencies on enthalpy, pressure, and shape. The expression for stagnation-point heat-transfer rate given by Detra, Kemp, and Riddell (ref. 12) and modified to

$$\dot{q} = (\text{const})\sqrt{\frac{p_o}{R}}\, H_t^{1.075} \tag{2}$$

was chosen because it agreed well with the earlier experimental data of Winkler and Sheldahl (ref. 13), shown in figure 4. These data were obtained in the same facility used in this investigation and with the same operating conditions. Further, equation (2) is convenient because total enthalpy and stagnation pressure are state properties that can be determined experimentally, thus allowing a theoretical stagnation-point heat-transfer rate to be calculated for each test. This normalization procedure will be shown to collapse each set of afterbody heat-transfer-rate data satisfactorily.

The experimental heat-transfer-rate data were compared with an analytical prediction, Lees' equilibrium heat-transfer-rate formula (ref. 14), for the afterbody of a hemisphere-cylinder

$$\frac{\dot{q}_w}{\dot{q}_o} = \frac{\frac{1}{2}\frac{p}{p_o}\left(\frac{u_e}{u_\infty}\right) r}{\left\{\frac{1}{u_\infty R}\left[\frac{du_e}{d(S/R)}\right]_o \int_o^S \frac{p}{p_o}\left(\frac{u_e}{u_\infty}\right) r^2\, dS\right\}^{1/2}} \tag{3}$$

To evaluate equation (3) along the afterbody, several assumptions were made. The static pressure was assumed to follow the modified Newtonian pressure distribution over the surface of the hemisphere but to be constant along the cylindrical afterbody:

$$\left.\begin{aligned} \frac{p}{p_o} &= \cos^2\left(\frac{S}{R}\right) + \frac{1}{\gamma M_\infty^2}\sin^2\left(\frac{S}{R}\right) && 0 \le \frac{S}{R} \le \frac{\pi}{2} \\ &= \text{constant} && \frac{S}{R} \ge \frac{\pi}{2} \end{aligned}\right\} \tag{4}$$

The Newtonian velocity gradient was assumed for the hemisphere, and u_e was taken as constant on the afterbody. The denominator of equation (3) was then evaluated in two parts, the first from the stagnation point to the shoulder of the hemisphere and the second commencing at the shoulder. With these assumptions and restrictions, equation (3) reduces to:

$$\frac{\dot{q}_w}{\dot{q}_o} = \frac{\frac{1}{2}\frac{p}{p_o}}{\left\{\frac{2}{\pi}\left[\frac{\pi}{32} + \frac{1}{\gamma M_\infty^2}\left(\frac{3\pi}{32} + \frac{1}{2\pi}\right) + \frac{p}{p_o}\left(\frac{S}{R} - \frac{\pi}{2}\right)\right]\right\}^{1/2}} \quad \text{for } \frac{S}{R} \geq \frac{\pi}{2} \tag{5}$$

The distributions shown in figure 5 result when a constant afterbody pressure distribution of $p/p_o = 0.030$, which approximates that measured experimentally (fig. 3), and an apparent isentropic exponent $\gamma = 1.45$ (as determined in ref. 7) are introduced into equation (5).

Figure 5(a) shows the data for afterbody heat-transfer rate on the uniformly catalytic copper-plated body. Since heat-transfer rates in equilibrium and frozen flow do not differ appreciably when the surface material is a good catalyst, it can be expected, as is shown on figure 5(a), that the theory would agree with the data for the test body completely covered with copper. Although some approximations were made in determining the theoretical distribution, the experimental data for the copper-wall test body do agree to within 15 percent with the theoretical distribution.

Figure 5(b) shows the heat-transfer rates to the afterbody behind the nose coated with noncatalytic silicon monoxide. Figure 5(b) demonstrates that when the highly concentrated reactant that accumulates in the boundary layer over the noncatalytic nose surface is recombined on the catalytic afterbody, the heat-transfer rate approximately doubles as compared with the calculated equilibrium distribution.

Figure 5(c) shows the data for the body completely covered with silicon monoxide. The heat-transfer rates measured on the afterbody lie below those predicted from Lees' analysis for equilibrium flow.

Figure 5(d) shows the data for the same afterbody as that used in figure 5(c) but with a catalytic copper nose. The nose surface material has no noticeable effect on measured afterbody heat-transfer rates over the silicon monoxide afterbody.

Figure 6 is a summary of figure 5. It shows that when the flow in the boundary layer is frozen, different values of surface catalytic activity on the nose increases the heat-transfer rate to the afterbody by different amounts when the afterbody surface material is a good catalyst. When the afterbody surface material is a poor catalyst, the catalytic activity of the nose surface has little effect on the heat transfer on the afterbody.

For the purpose of comparing the test results with the theoretical analysis of Chung et al. (ref. 6), it is required that the measured heat-transfer rate be separated into two portions: that due to convection, and that due to surface recombination. Neglecting radiation, the total heat-transfer rate to the test body is written as the sum of the convective and surface recombination heat-transfer rates:

$$\dot{q}_t = \dot{q}_c + \dot{q}_d \tag{6}$$

where

$$\dot{q}_d = \rho_w D_w \left(\frac{\partial \alpha}{\partial y}\right)_w h_r \tag{7}$$

Since

$$D_w \left(\frac{\partial \alpha}{\partial y}\right)_w = k_w \alpha_w \tag{8}$$

equations (7) and (8) together give

$$\dot{q}_d = \rho_w k_w \alpha_w h_r \tag{9}$$

for the surface recombination heat-transfer rate.

A comparison between the afterbody heat-transfer rates of the Cu-SiO model and the SiO-SiO model (fig. 6) indicates that the silicon monoxide surface has a specific reaction rate constant k_w very close to zero. This is deduced from the fact that a change in the nose material, which resulted in boundary layers with drastically different atom concentration gradients, $(\partial\alpha/\partial y)_w$, at $S/R = 2.682$ had no appreciable effect on the heat-transfer rate to the afterbody coated with silicon monoxide. Thus for the silicon monoxide surface the heat transfer is essentially convective.

It is fairly well established that clean oxygen-free copper has a high specific reaction rate constant (i.e., $k_w \to \infty$, refs. 1 and 13). Thus since $k_w \to \infty$ for the clean copper surface (i.e., $\alpha_w \to 0$) and $k_w \to 0$ for the silicon monoxide surface (i.e., $\alpha_w \to \alpha_e$), the heat transfer to the silicon monoxide surface is assumed to be purely convective so that

$$(\dot{q}_t)_{SiO\text{-}SiO} = (\dot{q}_c)_{SiO\text{-}SiO} + (\dot{q}_d)_{SiO\text{-}SiO} = \dot{q}_c \tag{10}$$

The heat-transfer rate to the copper surface, which has heat-transfer contributions due both to convective and to surface recombination processes, can in like manner be written:

$$(\dot{q}_t)_{Cu\text{-}Cu} = (\dot{q}_c)_{Cu\text{-}Cu} + (\dot{q}_d)_{Cu\text{-}Cu} \tag{11}$$

Equation (10) may then be subtracted from equation (11) to yield the rate of heat transfer to the copper surface due to surface recombination only, provided the rate of convective heat transfer to the silicon monoxide surface is the same as that to the copper surface. This procedure is justified because the stream energies are the same and the chemistry of the boundary layer is assumed to be frozen. The heat-transfer rate due to surface recombination for a uniformly catalytic body may then be evaluated from the measurements by means of the following equation:

$$\left.\begin{aligned} \dot{q}_d &= (\dot{q}_t)_{Cu\text{-}Cu} - (\dot{q}_t)_{SiO\text{-}SiO} \\ \text{or} \\ (\dot{q}_d)\ \text{uniformly catalytic body} &= (\rho_w k_w \alpha_w h_r)_{un} \end{aligned}\right\} \qquad (12)$$

When the nose material is noncatalytic and the afterbody material is catalytic, similar reasoning can be applied to yield measured values of the heat-transfer rate due to surface recombination for the configuration with a discontinuity in surface catalytic activity. The resulting equation is simply:

$$\dot{q}_d = \rho_w k_w \alpha_w h_r$$

Well-known relationships for the heat-transfer rate due to surface recombination can be used to formulate the theoretical predictions of reference 6 for comparison directly with the test results.

Letting

$$m_w = (\alpha/\alpha_e)_w$$

where the species concentration at the outer edge of the boundary layer, α_e, is a constant along the afterbody for a frozen boundary layer, the equation for surface recombination heat-transfer rate is then

$$\dot{q}_d = \rho_w k_w \alpha_e m_w h_r \qquad (13)$$

Dividing $\dot{q}_d$ by $(\dot{q}_d)_{un}$ gives the ratio of surface recombination heating for a nonuniformly catalytic body to that for a uniformly catalytic body:

$$\frac{\dot{q}_d}{(\dot{q}_d)_{un}} = \frac{\rho_w k_w \alpha_e m_w h_r}{(\rho_w k_w \alpha_e m_w h_r)_{un}} \qquad (14)$$

The surface static pressure is an extremely weak function of the surface material and is assumed to be the same for both cases,

$$P_w = \rho_w(1 + \alpha_w)RT_w = [\rho_w(1 + \alpha_w)RT_w]_{un} \qquad (15)$$

But over the short test times involved $T_w \simeq (T_w)_{un}$. Therefore, the ratio of wall densities becomes

$$\frac{\rho_w}{(\rho_w)_{un}} \cong \frac{(1 + \alpha_w)_{un}}{1 + a_w} \; ; \qquad \alpha_e = (\alpha_e)_{un} \qquad k_w \to \infty \qquad (16)$$

The atom mass fractions at the wall are unequal for the two bodies (i.e., $\alpha_w \neq (\alpha_w)_{un}$) but are small in comparison with unity.

Thus, with $\alpha_w \to 0$

$$\rho_w \cong (\rho_w)_{un} \tag{17}$$

This results in the relationship,

$$\frac{\dot{q}_d}{(\dot{q}_d)_{un}} \cong \frac{m_w}{(m_w)_{un}} \tag{18}$$

which relates the calculated species concentration at the wall with the measured surface recombination heat-transfer rates.

The theoretical results in reference 6 for the ratio $m_w/(m_w)_{un}$ are for a flat plate. Since the experimental data are for the afterbody of a hemisphere-cylinder, it is necessary to transform the flat-plate coordinates to hemisphere-cylinder coordinates to effect a valid comparison between theory and experiment. This is done by the inverse transformation used by Chung and Anderson (ref. 2).

$$x = \int_o^s C \frac{p}{p_o} u_e r^2 \, ds \tag{19}$$

Using the assumptions for pressure distribution and velocity gradient introduced earlier, the flat-plate coordinate x as a function of S/R becomes

$$x = C \frac{\pi}{2} R^3 \sqrt{\frac{2p_o}{\rho_o}} \left[(0.108) + 0.030 \left(\frac{S}{R} - \frac{\pi}{2} \right) \right] \tag{20}$$

As written, this equation is applicable only for $S/R \geq \pi/2$. The flat-plate coordinate x/x_1 of reference 6 is derived from equation (20) by normalizing with respect to the point of catalytic discontinuity.

The constant (Newtonian) value of velocity gradient is accurate on a hemisphere only for values of S/R less than 1.4. Part of the errors caused by the assumptions are cancelled by normalizing with x_1, the transformed coordinate distance to the point of catalytic discontinuity. Such errors can influence conclusions only with respect to the axial position at which catalytic phenomena may or may not occur, but they cannot alter the magnitude of such phenomena.

Figure 7 is a comparison of the experimental data with the theoretical results (ref. 6) for the conditions of a noncatalytic nose material and a catalytic downstream. The S/R coordinate has been normalized with S_1/R, where S_1 is the coordinate distance to the afterbody location of catalytic discontinuity. The theoretical ratio $\dot{q}_d/(\dot{q}_d)_{un}$ drops asymptotically to unity when

the boundary layer and surface reactions do not feel the existence of the noncatalytic upstream material. The data decrease with the analytic curve along the forward portion of the afterbody, but increase for S/S_1 greater than 2.5 instead of tending to unity. Why the experimental ratio of $\dot{q}_d/(\dot{q}_d)_{un}$ increases on the afterportion of the test body is not fully understood. A portion of the heat liberated by the surface reactions may have been incompletely accommodated by the copper wall, and this energy may have returned to the boundary layer and reappeared farther back on the afterbody in the form of additional convective heating. Thus data might not indicate a precise trend for the ratio of $\dot{q}_d/(\dot{q}_d)_{un}$ on the rearmost portion of the afterbody because they reflect an augmented heat-transfer rate due, in part, to convection. At least, they would not agree with the theory because the analysis does not allow for incomplete accommodation.

Figure 8 demonstrates the effect of a noncatalytic nose surface on the total heat-transfer rate to a catalytic afterbody by showing the variation of the ratio, $(\dot{q}_t)_{SiO\text{-}Cu}/(\dot{q}_t)_{Cu\text{-}Cu}$ with S/R. The total heat-transfer rate along the catalytic afterbody was increased when catalytic shielding was provided at the nose region. This total heat-transfer-rate ratio also increased on the rear portion of the afterbody, as did the ratio of heat-transfer rates due to surface recombinations shown in figure 7. Figure 8 indicates, for the test conditions encountered during the investigation, that the afterbody heat-transfer-rate distribution to a body with nose shielding is of the order of 50 percent higher than the corresponding distribution for a uniformly catalytic test body.

SUMMARY OF RESULTS

The effect that the catalytic activity of a surface material at the stagnation region of a flight vehicle may have on the laminar heat-transfer-rate distribution along the afterbody when the gas at the edge of the boundary layer is frozen in some nonequilibrium state has been examined experimentally. Laminar heat-transfer-rate distributions were measured along the afterbodies of hemisphere-cylinder models with various combinations of catalytic and noncatalytic upstream and downstream surface materials in streams of high enthalpy, partially dissociated nitrogen. It was found that the use of a noncatalytic surface material on the upstream portion of the body augments the heat-transfer rate on an afterbody that has a surface material with a finite catalytic activity. The results, compared with a uniformly catalytic test body, show that the use of noncatalytic material on the forward region of the body increases the heat-transfer rates to the catalytic afterbody surface by as much as 50 percent and when compared with a uniformly noncatalytic test body, the heat-transfer rates are increased by 300 percent to 400 percent. The results

of the experiment agree qualitatively with the analysis of Chung, Liu, and Mirels, but the experimental evidence indicates that augmented heat-transfer rates persist further downstream than theory predicts.

Ames Research Center
National Aeronautics and Space Administration
Moffett Field, Calif., June 16, 1966
129-01-09-06

REFERENCES

1. Goulard, Robert J.: On Catalytic Recombination Rates in Hypersonic Stagnation Heat Transfer. Jet Propulsion, vol. 28, no. 11, Nov. 1958, pp. 737-745.

2. Chung, Paul M.; and Anderson, Aemer D.: Heat Transfer to Surfaces of Finite Catalytic Activity in Frozen Dissociated Hypersonic Flow. NASA TN D-350, 1961.

3. Chambré, Paul L.; and Acrivos, Andreas: On Chemical Surface Reactions in Laminar Boundary Layer Flows. J. Appl. Phys., vol. 27, no. 11, Nov. 1956, pp. 1322-1328.

4. Rosner, Daniel E.: Diffusion and Chemical Surface Catalysis in Flow Systems. Tech. Pub. No. 14. AeroChem Research Labs., Inc., Princeton, N.J., Sept. 1959.

5. Inger, George R.: Nonequilibrium Stagnation Point Boundary Layers with Arbitrary Surface Catalycity. AIAA J., vol. 1, no. 8, Aug. 1963, pp. 1776-1784.

6. Chung, P. M.; Liu, S. W.; and Mirels, H.: Effect of Discontinuity of Surface Catalycity on Boundary Layer Flow of Dissociated Gas. Rep. TDR-69 (2240-20)TN-1. Aerospace Corp., El Segundo, Calif., June 1962.

7. Winkler, Ernest L.; and Griffen, Roy N., Jr.: Effects of Surface Recombination on Heat Transfer to Bodies in a High Enthalpy Stream of Partially Dissociated Nitrogen. NASA TN D-1146, 1961.

8. Winkler, Ernest L.; and Griffen, Roy N., Jr.: Measurements in a Frozen, Partially Dissociated, High-Speed Gas Stream. Proc. Second Symposium on Hypervelocity Techniques, Univ. of Denver, Denver Res. Inst., Plenum Press, N.Y., 1962, pp. 511-522.

9. Manos, William P.; and Taylor, Donald E.: Analysis of Interpretation of Data on Thin-Skinned Heat-Transfer Models. J. Heat Transfer (Trans. ASME, vol. 84, ser. C, no. 2) May 1962, pp. 191-192.

10. Inouye, Mamoru; Rakich, John, V.; and Lomax, Harvard: A Description of Numerical Methods and Computer Programs for Two-Dimensional and Axisymmetric Supersonic Flow Over Blunt-Nosed and Flared Bodies. NASA TN D-2970, 1965.

11. Potter, J. Leigh; Kinslow, Max; and Boylan, David E.: An Influence of the Orifice on Measured Pressures in Rarefied Flow. AEDC-TDR-64-175, ARO Inc., Arnold Air Force Station, Tenn., Sept. 1964.

12. Detra, R. W.; Kemp, N. H.; and Riddell, F. R.: Addendum to Heat Transfer to Satellite Vehicles Re-entering the Atmosphere. Jet Prop., vol. 27, no. 12, Dec. 1957, pp. 1256-1257.

13. Winkler, Ernest L.; and Sheldahl, Robert E.: Influence of Calorimeter Surface Treatment on Heat-Transfer Measurements in Arc-Heated Test Streams. AIAA J., vol. 4, no. 4, April 1966, pp. 715-716.

14. Lees, Lester: Laminar Heat Transfer Over Blunt-Nosed Bodies at Hypersonic Flight Speeds. Jet Prop., vol. 26, no. 4, April 1956, pp. 259-269.

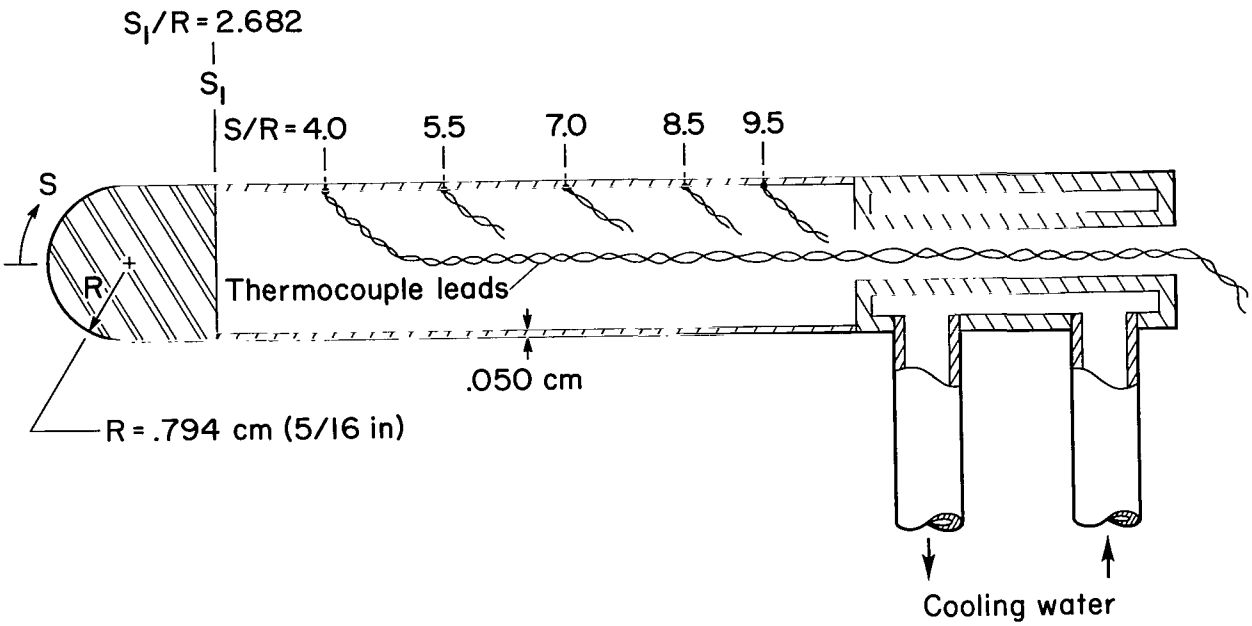

(a) Afterbody heat-transfer rate test body.

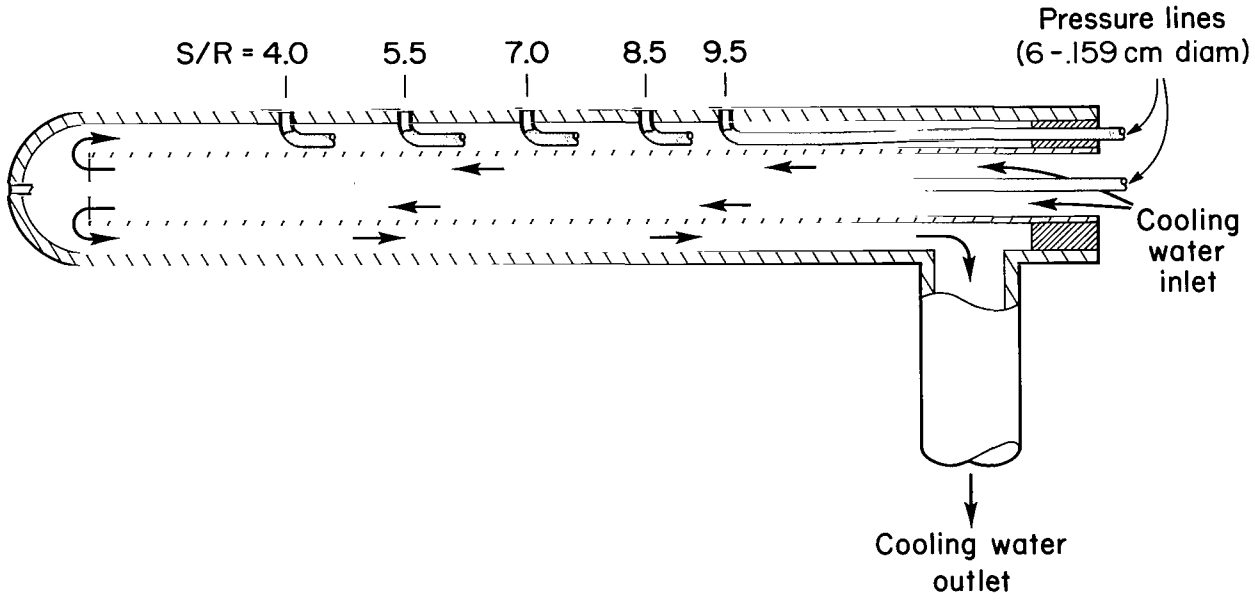

(b) Stagnation-point and afterbody pressure test body.

Figure 1.- Test bodies.

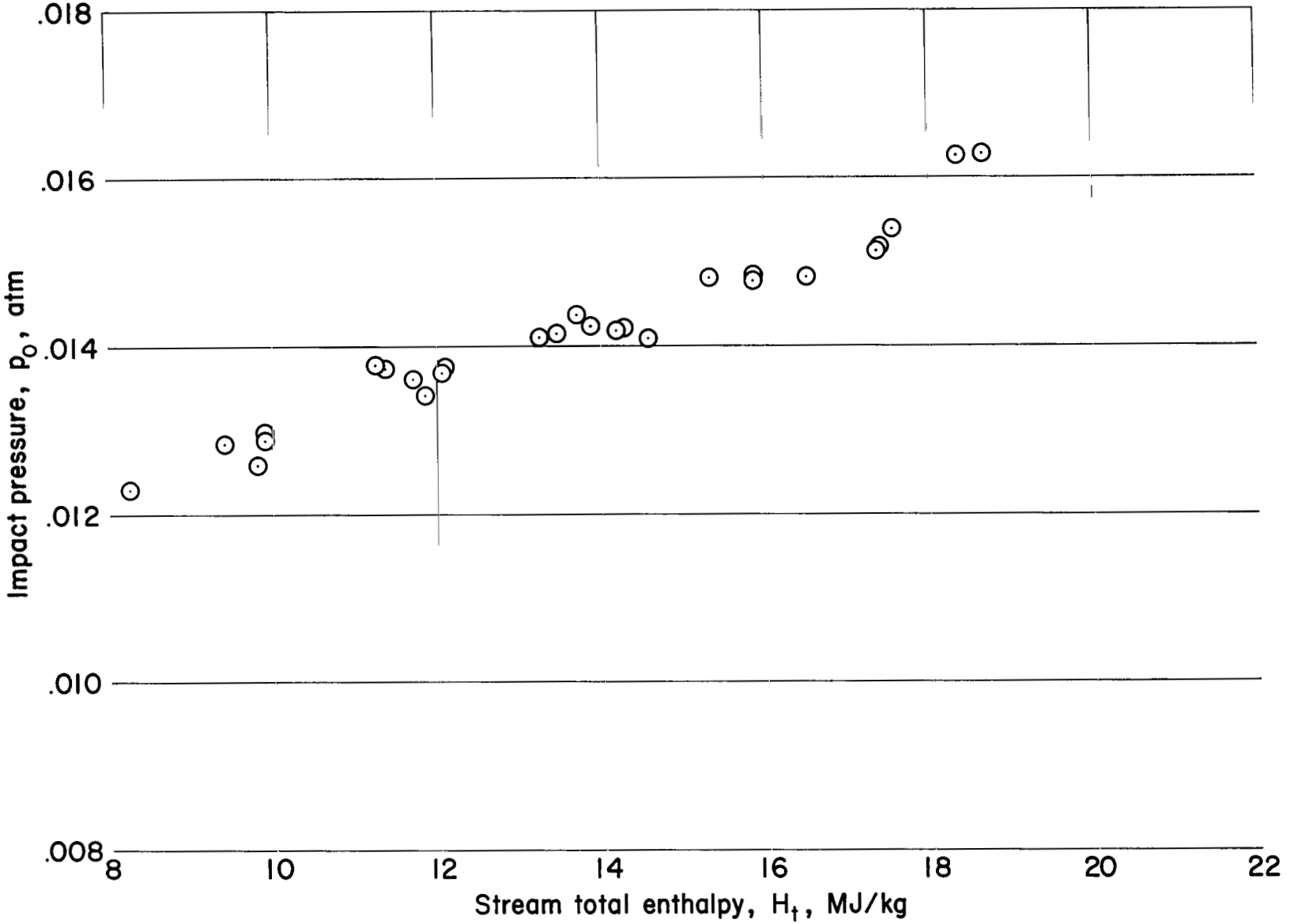

Figure 2.- Impact pressure versus test stream total enthalpy in arc-heated nitrogen streams.

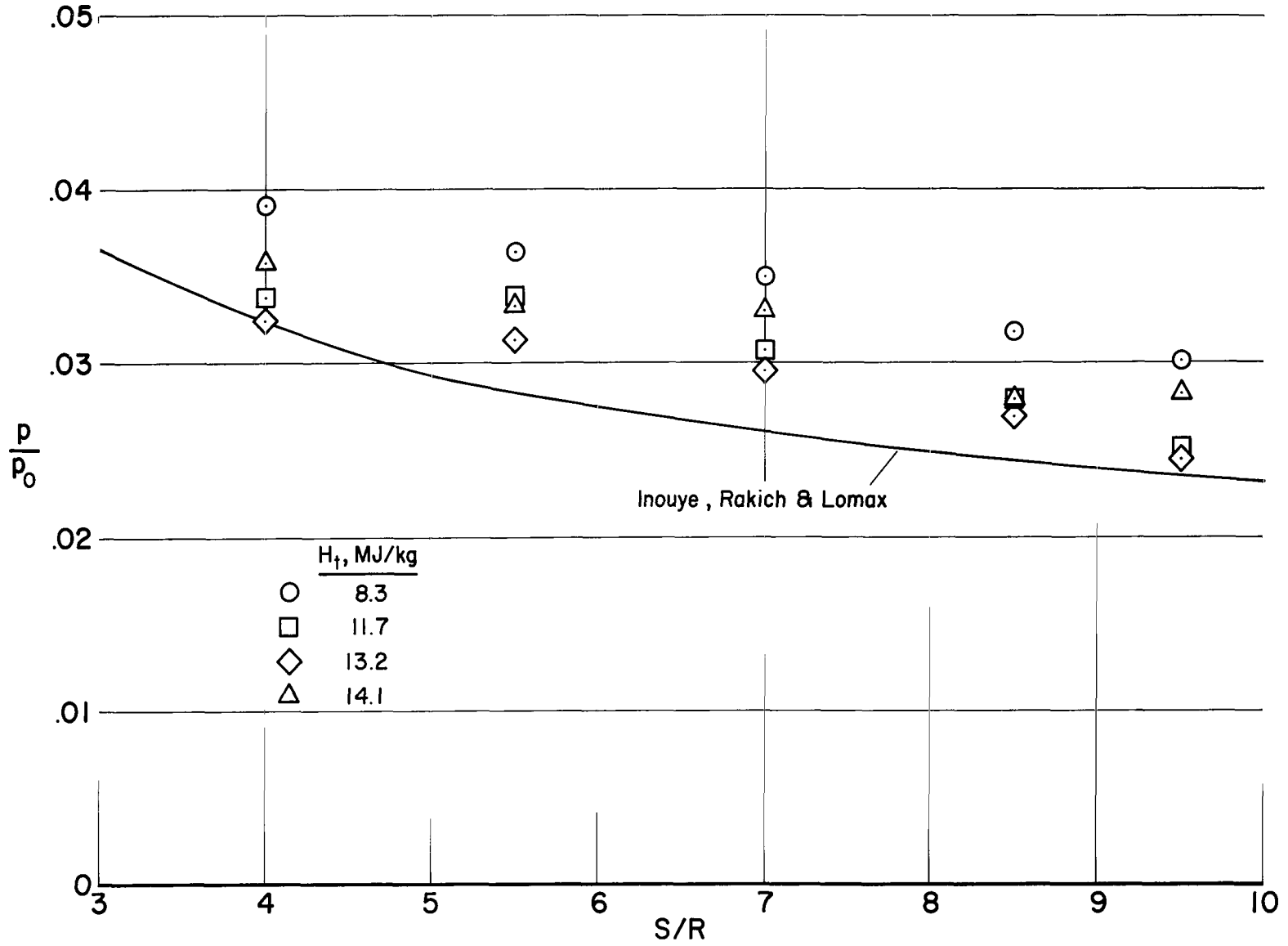

Figure 3.- Afterbody pressure distribution over a 1.588-cm-diameter hemisphere-cylinder in arc-heated nitrogen streams at Mach 5.6.

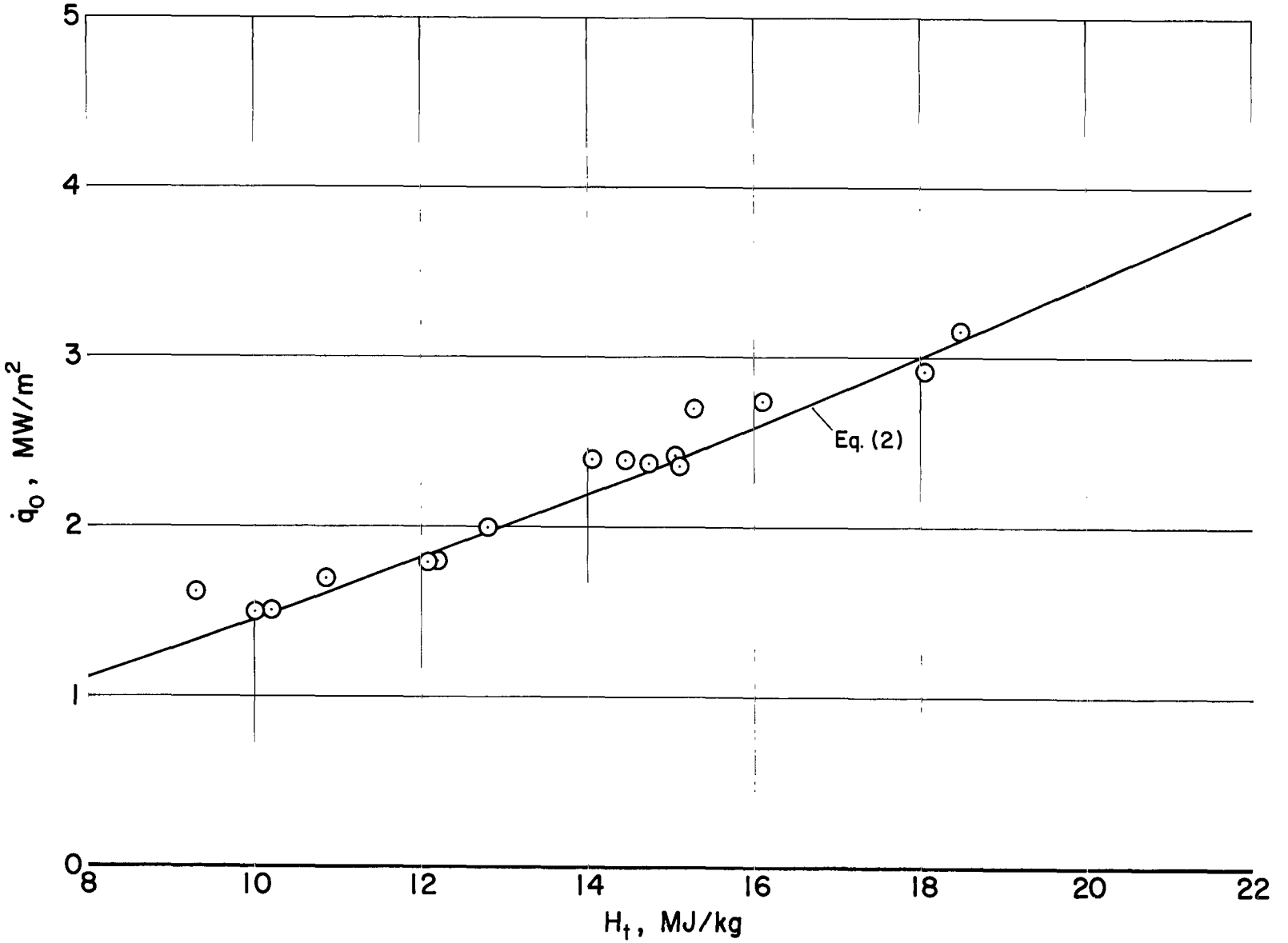

Figure 4.- Stagnation-point heat-transfer rates to a 0.794 cm (5/16 in.) nose radius test body in arc-heated nitrogen streams.

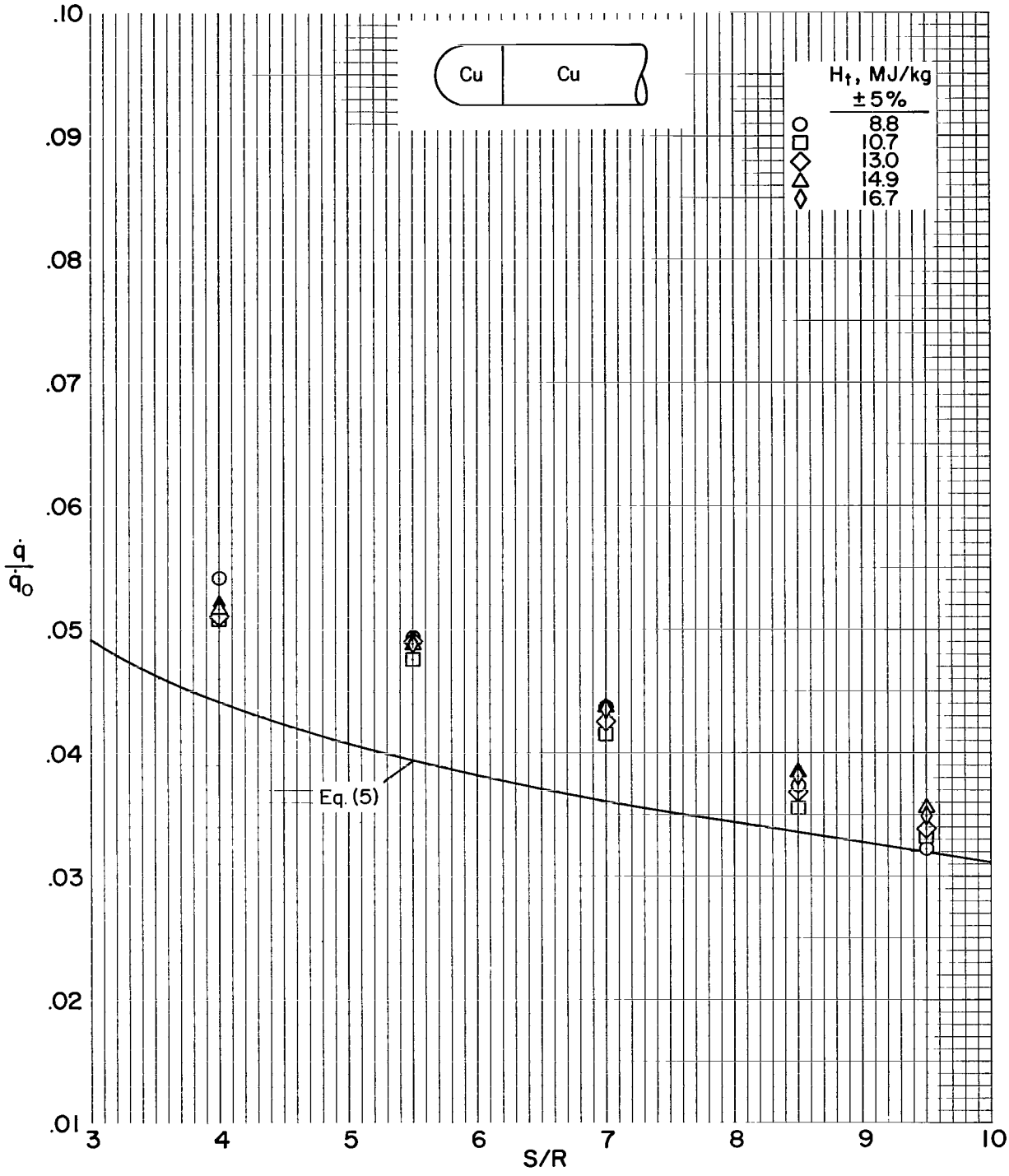

(a) Cu-Cu test body.

Figure 5.- Normalized afterbody heat-transfer rates to test bodies in arc-heated nitrogen streams.

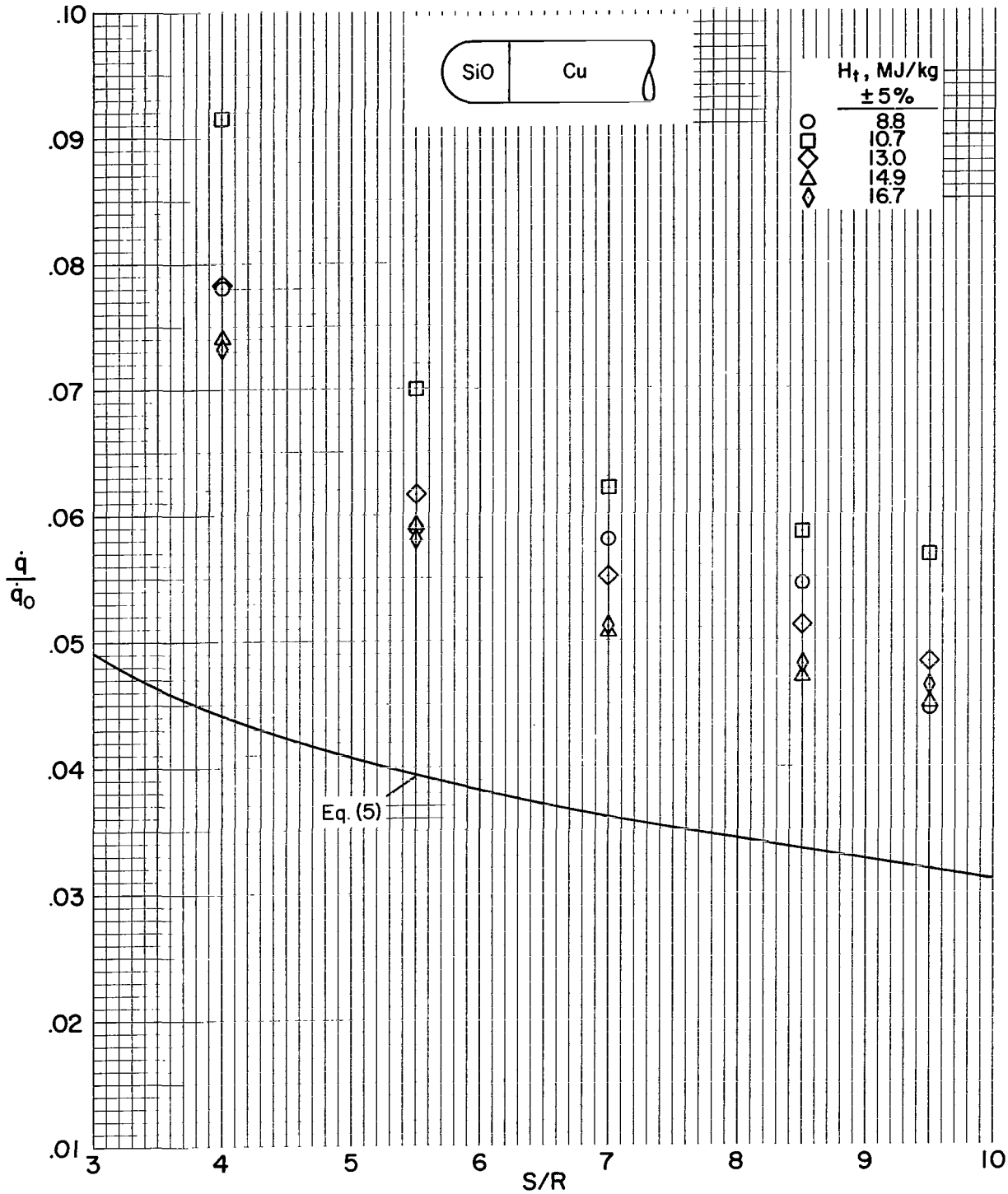

(b) SiO-Cu test body.

Figure 5.- Continued.

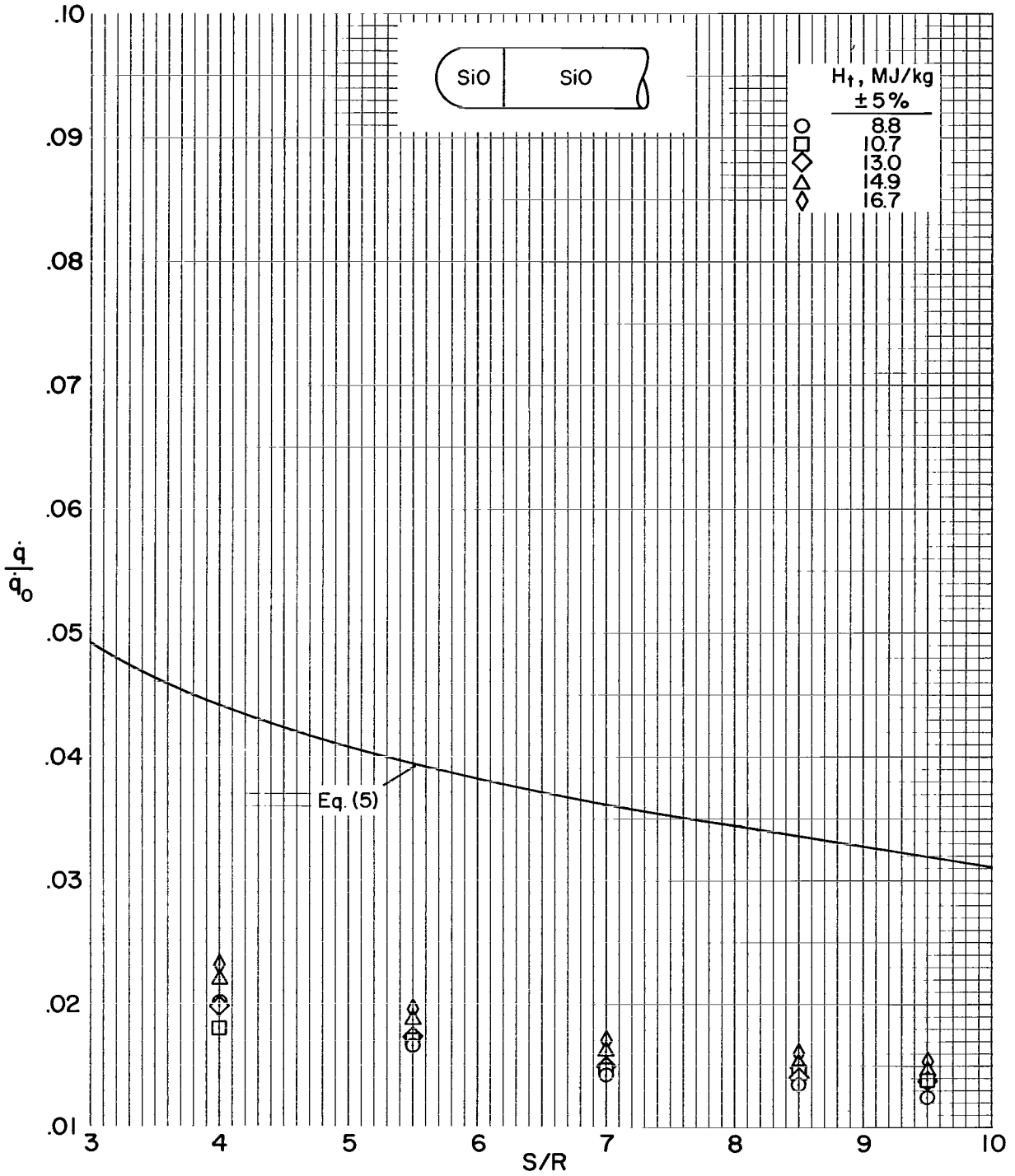

(c) SiO-SiO test body.

Figure 5.- Continued.

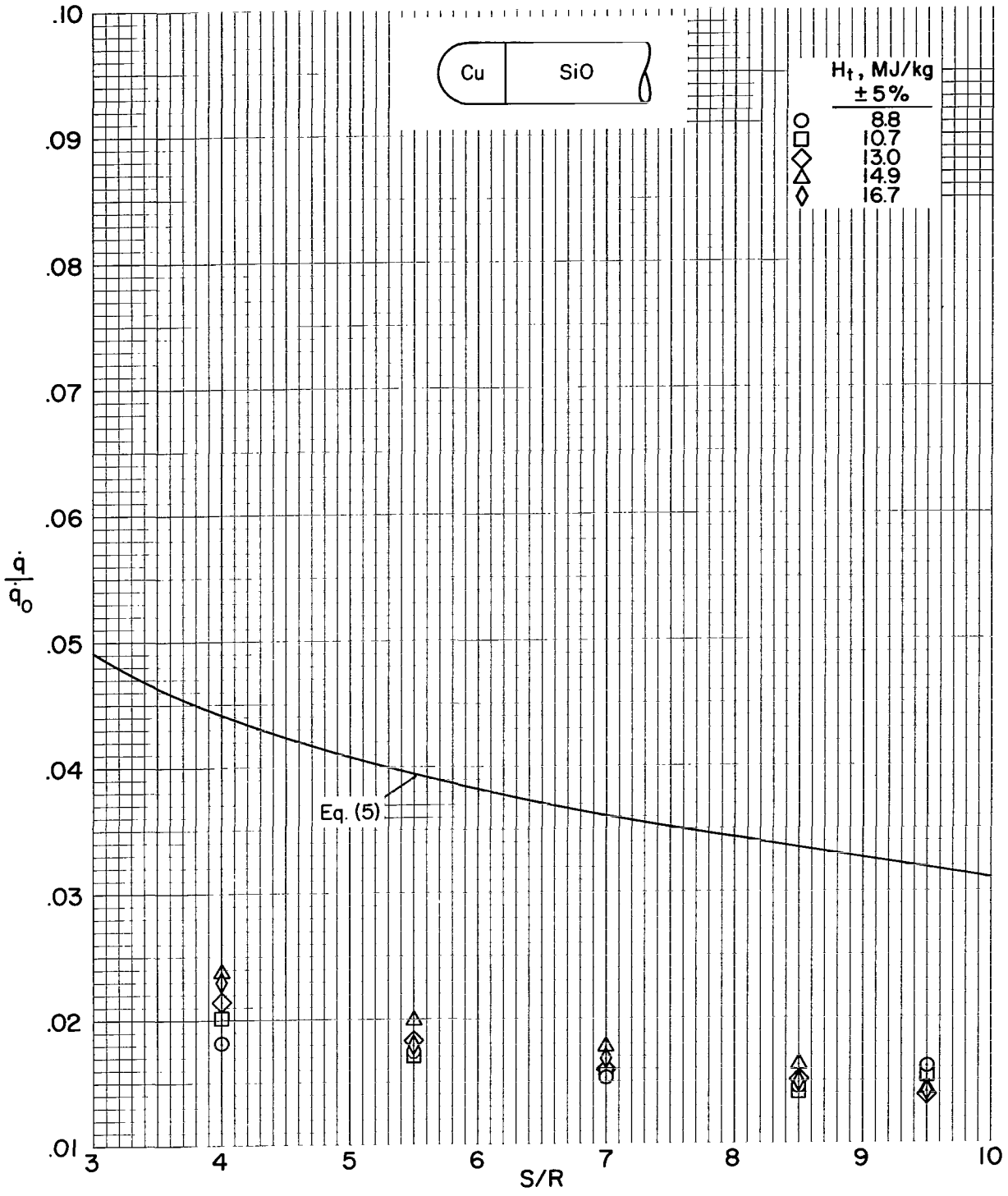

(d) Cu-SiO test body.

Figure 5.- Concluded.

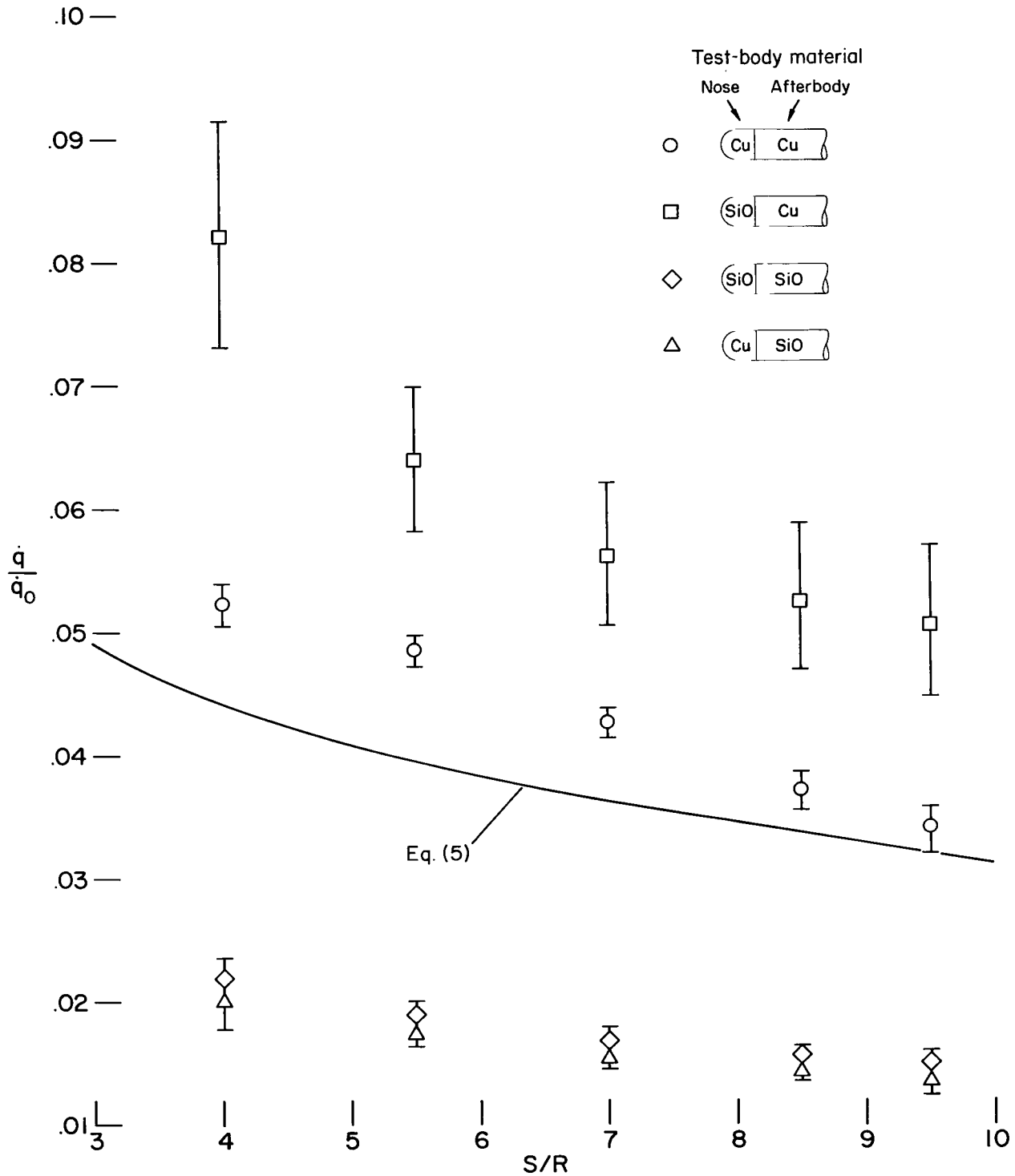

Figure 6.- Normalized afterbody heat-transfer rates to bodies with various catalytic discontinuities.

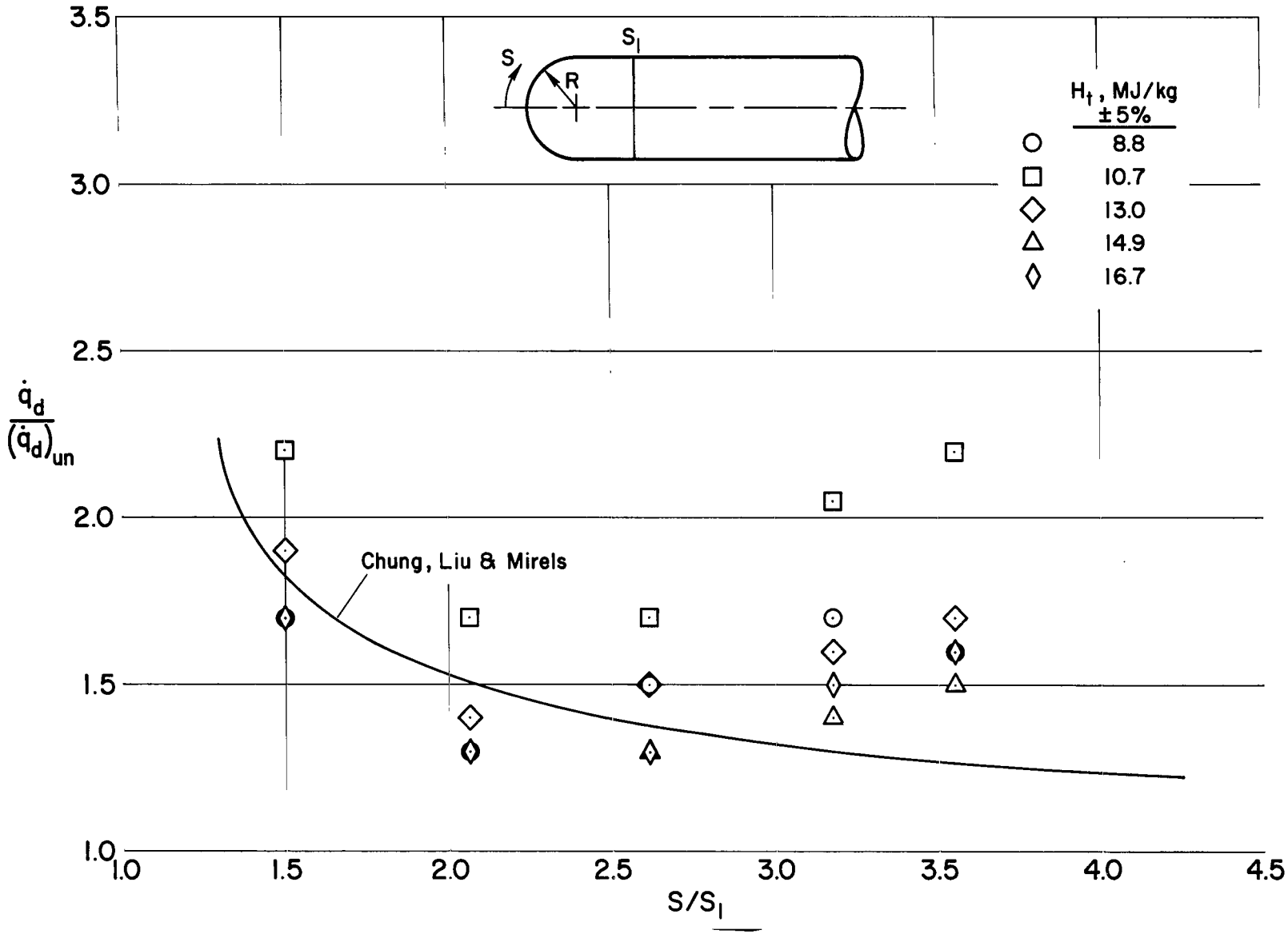

Figure 7.- Ratio of surface-recombination heat-transfer rates on the afterbody of a test body with a SiO coated nose and Cu coated afterbody to that of a uniformly Cu coated test body as a function of normalized afterbody position.

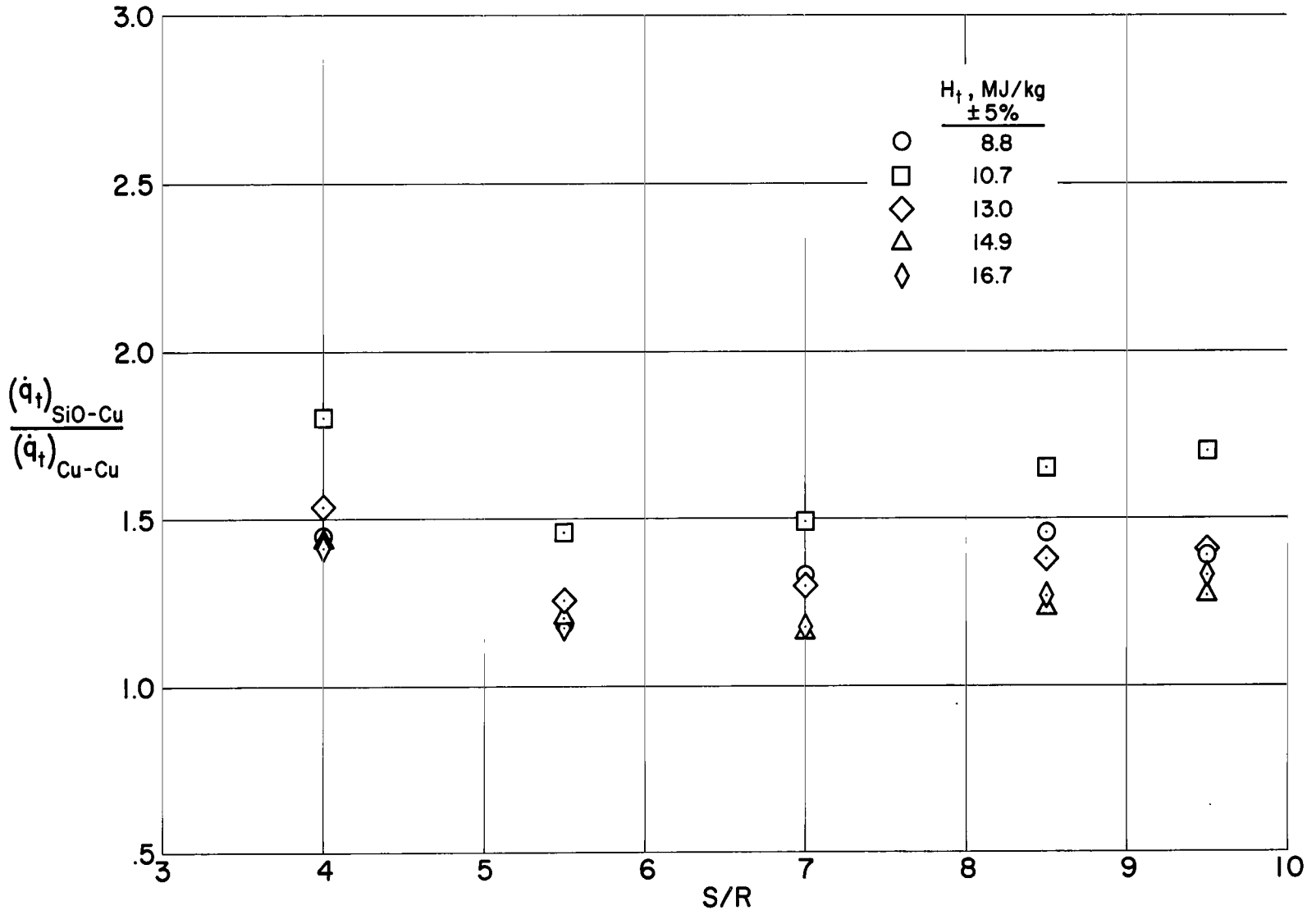

Figure 8.- Ratio of heat-transfer rates on the afterbody of a test body with a SiO coated nose and Cu coated afterbody to that of a uniformly coated copper test body as a function of afterbody location.

"The aeronautical and space activities of the United States shall be conducted so as to contribute . . . to the expansion of human knowledge of phenomena in the atmosphere and space. The Administration shall provide for the widest practicable and appropriate dissemination of information concerning its activities and the results thereof."

—NATIONAL AERONAUTICS AND SPACE ACT OF 1958

NASA SCIENTIFIC AND TECHNICAL PUBLICATIONS

TECHNICAL REPORTS: Scientific and technical information considered important, complete, and a lasting contribution to existing knowledge.

TECHNICAL NOTES: Information less broad in scope but nevertheless of importance as a contribution to existing knowledge.

TECHNICAL MEMORANDUMS: Information receiving limited distribution because of preliminary data, security classification, or other reasons.

CONTRACTOR REPORTS: Technical information generated in connection with a NASA contract or grant and released under NASA auspices.

TECHNICAL TRANSLATIONS: Information published in a foreign language considered to merit NASA distribution in English.

TECHNICAL REPRINTS: Information derived from NASA activities and initially published in the form of journal articles.

SPECIAL PUBLICATIONS: Information derived from or of value to NASA activities but not necessarily reporting the results of individual NASA-programmed scientific efforts. Publications include conference proceedings, monographs, data compilations, handbooks, sourcebooks, and special bibliographies.

Details on the availability of these publications may be obtained from:

SCIENTIFIC AND TECHNICAL INFORMATION DIVISION

NATIONAL AERONAUTICS AND SPACE ADMINISTRATION

Washington, D.C. 20546